Published in final edited form as:
*J Biomed Mater Res A*. 2013 September ; 101(9): 2559–2572. doi:10.1002/jbm.a.34565.

# Neural Responses to Electrical Stimulation on Patterned Silk Films

**Marie Hronik-Tupaj**[1], **Waseem Khan Raja**[1], **Min Tang-Schomer**[1], **Fiorenzo G. Omenetto**[1], and **David L. Kaplan**[1,*]

[1]Department of Biomedical Engineering, 4 Colby Street, Science & Technology Center, Tufts University, Medford, MA 02155 USA

## Abstract

Peripheral nerve injury is a critical issue for trauma patients. Following injury, incomplete axon regeneration or misguided axon innervation into tissue will result in loss of sensory and motor functions. The objective of this study was to examine axon outgrowth and axon alignment in response to surface patterning and electrical stimulation. To accomplish our objective, metal electrodes with dimensions of 1.5 mm × 4 cm, were sputter coated onto micropatterned silk protein films, with surface grooves 3.5 μm wide × 500 nm deep. P19 neurons were seeded on the patterned electronic silk films and stimulated at 120 mV, 1 kHz, for 45 minutes each day for 7 days. Responses were compared to neurons on flat electronic silk films, patterned silk films without stimulation, and flat silk films without stimulation. Significant alignment was found on the patterned film groups compared to the flat film groups. Axon outgrowth was greater ($p < 0.05$) on electronic films on day 5 and day 7 compared to the unstimulated groups. In conclusion, electrical stimulation, at 120 mV, 1 kHz, for 45 minutes daily, in addition to surface patterning, of 3.5 μm wide × 500 nm deep grooves, offered control of nerve axon outgrowth and alignment.

### Keywords

neuron; silk; biomaterial; electrical stimulation; tissue engineering

## Introduction

Peripheral nerve regeneration is a critical issue as 2.8% of trauma patients present with this type of injury.[1] Causes for peripheral nerve injuries include violence, sports injuries, motor vehicle accidents, and tumor resection.[2] During a time of war, 14–18% of injuries affect the peripheral nervous system altering both sensation and muscle function.[3] Clinical options for

*Corresponding Author: david.kaplan@tufts.edu.
Contact Information:

1. Marie Hronik-Tupaj, Department of Biomedical Engineering, 4 Colby Street, Science & Technology Center, Tufts University, Medford, MA 02155 USA, telephone: (781) 330 -6907, fax: (617) 627 - 3231, marie.tupaj@gmail.com
2. Waseem Khan Raja, Department of Biomedical Engineering, 4 Colby Street, Science & Technology Center, Tufts University, Medford, MA 02155 USA, telephone: (617) 627 - 2641, fax: (617) 627 - 3231, waseem.raja@tufts.edu
3. Min Tang-Schomer, Department of Biomedical Engineering, 4 Colby Street, Science & Technology Center, Tufts University, Medford, MA 02155 USA, telephone: (617) 627 - 2641, fax: (617) 627 - 3231, min.tang-schomer@tufts.edu
4. Fiorenzo G. Omenetto, Department of Biomedical Engineering, 4 Colby Street, Science & Technology Center, Tufts University, Medford, MA 02155 USA, telephone: (617) 627 - 4972, fax: (617) 627 - 3231, fiorenzo.omenetto@tufts.edu
5. David L. Kaplan, Department of Biomedical Engineering, 4 Colby Street, Science & Technology Center, Tufts University, Medford, MA 02155 USA, telephone: (617) 627 - 3251, fax: (617) 627 - 3231, david.kaplan@tufts.edu

such injuries have changed only slightly in the last 30 years, with standard methods of treatment including suturing damaged nerve ends, grafting sensory nerves, and nerve transfers, with autografts as the gold standard.[4] Despite current treatments, only 10% of the patients regain complete functional recovery.[5]

Recent strategies investigated for repairing nerves include: (1) the addition of nerve growth factors, (2) stem cell and glial cell transplantation, (3) gene therapy, (4) functional electrical stimulation, and (5) natural and synthetic guidance channels.[6–10] In addition, surface topographies, ranging from the nanometer to micrometer scale, such as grooves, aligned fibers, roughness, and pores, have been identified to help direct and align nerve cells.[11–18] It is also known that electric fields have an impact on cell adhesion, proliferation, and differentiation[19–28] and have been utilized to increase axon outgrowth, accelerate axon repair, and increase muscle reinnveration.[29–31] Furthermore, a combination of strategies, such as multiple growth factors, electrical stimulation with gene transfer, and implanted stem cells as an adjuvant therapy with growth factors, have been utilized for the improved recovery of injured nerves.[32–34]

Various types of synthetic and natural materials have been studied in the field of biomedical engineering to improve tissue growth, ability, and regeneration[35–37], and silk biomaterial has demonstrated biocompatibility with peripheral nervous tissue repair.[38–44] Silk can be processed into many material formats such as scaffolds, films, gels, fibers, hollow tubes and microstructures[45–48] and is fully degradable to amino acids, thus avoiding complications such as nerve compression and chronic inflammation. Silk can be formed into materials with good mechanical strength and flexibility for regenerative medicine needs, including conformal bio-integrated electronics to fit curvilinear tissues in the central nervous system.[49]

In the present study, silk from the *Bombyx mori* silkworm was used. This silk is composed of a heavy chain fibroin approximately 391 kDa, and a light chain fibroin 27 kDa, held together by a disulfide bond, with glue-like proteins termed sericins that bind the fibers.[50,51] Our objective was to incorporate electrodes and surface topographies on flexible silk substrates to assess the combined effects of patterning and electrical stimulation on axon alignment and axon outgrowth. In addition, we demonstrate methods for depositing electronic components onto flexible silk films with morphologically patterned surfaces.

## Results and Discussion

### Electronic Patterned Silk Film Fabrication

Electronic patterned silk films were fabricated by a micro-molding technique with varying micropatterned surface topographies, electrode dimensions, pattern vs. electrode orientation, and electrode material. [M1]Surface topographies consisted of an array of grooves with the dimensions of 40 μm wide, 3.5μm having a 350 nm depth, and 3.5 μm wide grooves having a 500 nm depth (Figure 1A). Line electrodes with the dimensions of 0.5 mm × 4.0 mm, 1.0 mm × 4.0 mm, and an 8.0 mm × 50 μm electrode array with 2 $mm^2$ electrode pads were deposited both on flat and patterned silk films (Figure 1B). Electrode surface area was chosen based on unit isolation and the electrode width required to sputter through the depth of the mask.[52] Electrodes were oriented perpendicular, parallel, and at 45° from the silk film patterns (Figure 1C). Platinum/palladium, titanium, and gold materials were sputtered coated on 90 μm thick silk films (thickness measurements not shown) (Figure 1D). Sputtering was performed in assistant with a shadow mask, which allowed successful transfer of functional electrodes onto flexible surfaces with microscale topography. These methods can be accomplished at room temperature without the use of any harsh chemicals that do not alter the protein structure of the biomaterial. These thin silk films were mechanically stable that they survived all these processing conditions and cell culture procedures.

Several studies have incorporated inorganic materials with silk for applications in biomedical, optoelectronics, and photonics.[53–55] In our studies, gold, titanium, and platinum/palladium electrodes were chosen due to these material's well known biocompatible and conductive properties. Silk was used as our neuro-electronic substrate as it is a natural, biocompatible block copolymer with controllable degradation rates and controllable mechanical properties. Our patterned gold electronic silk films were transparent for imaging purposes and flexible for the purpose of future incorporation into functionalized nerve conduits.

Pattern dimensions were chosen based on what has been previously used in our lab for successful alignment of corneal fibroblasts on silk films.[56] In these prior studies, groove widths ranging from 445–3582 nm and groove depths ranging from 37–342 nm were tested and it was found that the groove depth had a larger effect on cell alignment than the groove width. [56] Our silk films patterns containing 3.5 μm groove widths and 500 nm depths closely followed these dimensions.

## Conductivity of Electronic Patterned Silk Films

Silk films were conductive down the length of each electrode when a 1 V test signal was applied. Crosstalk was not observed among the neighboring electrodes (Figure 2A – 2E). Twenty-five areas, specifically 5 areas per electrode and 5 electrodes per silk film were chosen and tested for electric conductivity (Figure 2F). Electrodes sputtered 25 nm thick on flexible silk films exhibited little to no conductivity. Electrodes 75 nm thick were 88.8 ± 2.54%, 86.2 ± 3.97%, and 91.7 ± 0.01% conductive at 1 V, 1 V 20 Hz, and 1 V 1 kHz, respectively (Figure 3B). For example, an average of 90.0% conductive can be explained as 90 out of every 100 electrodes were functional. Three different frequencies were tested due to the capacitive effect at the electrode-electrolyte interface. Electrodes with a thickness of 100 nm were 90.2 ± 1.1%, 91.3 ± 0.03%, and 91.6 ± 0.02% conductive at 1 V, 1 V 20 Hz, and 1 V 1 kHz, respectively (Figure 3B ). Conductivity of electrodes that were 75 nm thick and 100 nm thick was statistically higher ($p < 0.05$) than the conductivity of electrodes with a 25 nm thickness. Images of electrodes deposited on patterned silk films with 25 nm, 75 nm, and 100 nm thicknesses are shown in Figure 3A. Differences in electrode thickness are noted by the color differences of the electrodes in the figures.

Conductivity of electronic silk films was monitored following hydration. As a baseline measurement, electrodes deposited on silk films were 91.1 ± 5.16%, 99.6 ± 4.10%, and 99.9 ±0.0% conductive at 1 V, 1 V 20 Hz, and 1 V 1 kHz, respectively, prior to hydration. One day following hydration the electrodes were 69.7 ±11.9%, 79.9 ±8.71%, and 84.9 ± 8.19% conductive at 1 V, 1 V 20 Hz, and 1 V 1 kHz, respectively. At 2 days, electrodes were 75.5 ± 9.7%, 81.3 ± 9.41%, and 84.9 ± 8.20% conductive at 1 V, 1 V 20 Hz, and 1 V 1 kHz, respectively. At 7 days, electrodes were 60.1 ± 0.01%, 89.8 ± 6.87%, and 90.3 ± 6.57% conductive at 1 V, 1 V 20 Hz, and 1 V 1 kHz, respectively. At 14 days, electrodes were 40.0 ± 0.01%, 56.9 ± 10.3%, and 68.6 ± 9.40% conductive at 1 V, 1 V 20 Hz, and 1 V 1 kHz, respectively. Statistical differences ($p < 0.05$) between the conductivity of hydrated electrodes and the conductivity of electrodes prior to hydration were at 2 weeks for all groups (Figure 4A). Therefore, cultures were maintained for 7 days.

The metal electrodes bonded to the 90 μm thick, flexible patterned silk fibroin films in a hydrated environment. Decreases in conductivity were observed as the silk films degraded in a hydrated environment over two weeks (Figure 4A). Silk degradation time in water was dependent upon beta-sheet content and film thickness.[57,58] Insulation between electrodes was only tested and reported following electronic film fabrication (Figure 2). As the films degraded the gold electrodes dispersed, resulting in a degradable device. These parameters can be tailored for the amount of treatment time needed in an *in vivo* environment.

### Functional Material Interfaces

Different materials were utilized to form the functional electronic material interfaces, including e-gel, silver paste, and silicon glue. Both the e-gel and the silver paste were options in attaching external electronics to the silk e-films. The e-gel interface (Figure 3D) was 78.2 ± 8.26%, 80.8 ± 8.5%, and 81.1 ± 8.38% conductive and the interface with chamber was 57.7± 11.3%, 67.0 ± 10.5% and 71.7 ± 7.36% conductive at 1 V, 1 V 20 Hz, 1V 1 kHz, respectively. The silver interface (Figure 3D) was 74.8 ± 9.92%, 84.9 ± 8.20%, and 89.9 ± 6.88% and with chamber was 84.8 ± 8.18%, 89.9 ± 6.89% and 74.8 ± 9.92% conductive at 1 V, 1 V 20 Hz, and 1 V 1 kHz, respectively. Conductivity between the electronic silk film interface and the electronic silk film interface with polydimethylsiloxane (PDMS) chamber groups did not show significant differences ($p < 0.05$) (Figure 3D).

While e-gel is not conductive it is a strong adhesive and is biocompatible.[59] Silver paste is conductive, though not adequate as a strong adhesive. Silicon glue may also be used as a non-conductive, biocompatible, strong adhesive[60], and was utilized with silver paste to secure the bond. Combinations of these materials are an option for optimizing conductivity and attachment.

### COMSOL Modeling

An image of the silk film with electrodes, PDMS chamber, and tissue culture dish that was utilized in the studies and modeled is shown in Figure 5A. Figure 5B shows a model of the electric potential at the anode, cathode and across the electronic silk film. Figure 5C shows the direction and magnitude of the electric field on the film. As can be seen from the field lines the strength of electric filed is strong between the electrodes and weaker away from the electrodes (Figure 5C). Any irregular field distribution was due to differences between the electrodes in contact with the culture media compared with the electrode in contact with the PDMS well. Electric field strength between the electrodes was 18.5 mV/mm. Field strength was comparable to prior studies utilizing electric fields for bone differentiation, cartilage repair and neural tissue engineering.[19,24,61,62]

### Cell Viability on Electronic Patterned Silk Films

P19 stem cells seeded at 5,000 cells/cm$^2$ attached and proliferated on 1 mM laminin coated gold e-films, 1 mM laminin coated platinum and palladium e-films, 1 mM laminin coated titanium e-films, and 1 mM laminin coated non-electrode silk films on day 1, day 3, day 5, and day 7. All groups increased in cell number between days 1, 3, 5, and 7 (Figure 4B). Specifically, p19 stem cells seeded on the gold electrodes increased 5.06 times over a 7 day culture period, 5.04 times on titanium, 5.66 times platinum/palladium and 4.82 times on silk films without electrodes.

### Axon Alignment on Electronic Patterned Silk Films

Fluorescent images of the p19 neuron axon alignment on flat silk films without stimulation, flat electronic silk films, patterned silk films without stimulation, and patterned electronic silk films are presented on days 1, 3, 5, and 7 (Figure 6). Directions of film patterns are noted by red arrows. Axons aligned with these film patterns are distinguished by the white arrows. Since neurons were stained with calcein acetoxymethyl ester (calcein AM), a polyanionic dye that is retained in live cells, all of the cells that were imaged were living. Differences in average axon alignment with the grooves were found between the patterned silk films and the flat silk films at all time points ($p < 0.05$) (Figure 7A). Differences between axon alignment on the patterned films with and without electrodes were found on days 3, 5, and 7 ($p < 0.05$) (Figure 7A). Quantification of axon alignment in all groups are reported within every 10 degrees (i.e., 0–10°, 10–20°, 20–30°, 30–40°, 40–50°, 50–60°, 60–

70°, 70–80°, 80–90°) from the groove on day 1 (Figure 7B), day 3 (Figure 7C), day 5 (Figure 7D) and day 7 (Figure 7E). The percentage of neurons on patterned films that are aligned within 0 – 20 degrees of the groove increased from 75.8% to 99.9% on days 1 to 7. The percentage of neurons on patterned electronic films that are aligned 0 - 20 degrees from the groove were 81.4% aligned on day 1 and 67.7% on day 7. The neurons on the flat groups were 35.3%, 26.5%, 28.5% and 16.6% aligned on days 1, 3, 5, and 7, respectively. The neurons on the flat electronic groups were 20.7%, 40%, 34.4%, and 23.4% aligned on days 1, 3, 5, and 7.

The patterned electronic films were comparable in alignment to the patterned films the day after plating (day 1), however, axon alignment, 0 -10 degrees from the groove, in the patterned electronic films decreased on day 3 from 48.1% to 35.6% while the patterned films without electrical stimulation increased from 44.8% to 54.3%. Here, the contribution of the electric field towards axon alignment is unknown. While direct currents have been demonstrated to align cells perpendicular to the electric fields[28,63–65], there have not been extensive reports examining the effects of alternating current stimulation on cell alignment. The effect of electrode orientation, electrode spacing, and electrode thickness on topographical surface for axon alignment or outgrowth will be a topic for future investigation.

### Axon Outgrowth on Electronic Patterned Silk Films

Cells revealed β3-tubulin protein expression in all groups on days 1, 3, 5, and 7 (Figure 8A). β3-tubulin, also known as tuj-1, encodes for a structural protein found in neuron axons and cytoskeleton, is expressed in microtubules and is a common marker for identifying nerve tissue.[66–68] Axon outgrowth in the flat, patterned, flat electronic, patterned electronic groups increased from days 1 to 3 following seeding on silk films (Figure 8A, 8B). Increased axon diameter was also observed in all groups between days 1 and 3. On days 5 and 7 there were statistical differences ($p < 0.05$) in axon length between the patterned films and the flat silk film groups with and without stimulation. Cells in the stimulated groups exhibited the greatest average axon length on day 5, compared to the unstimulated groups that exhibited the greatest average axon length on day 3. Differences in surface topography, either on the stimulated or unstimulated groups, did not affect ($p < 0.05$) average axon length. Immunostaining was compared to a negative control of non-differentiated p19 stem cells (data not shown). Since p19 neurons are morphologically similar to that of cortical neurons, dendrites are typically not observed following neural differentiation. Thus, when measuring outgrowth, a distinction was not made between different processes.

Neural stem cell lines are popular in *in vitro* studies that examine the effects of electrical stimulation in neural tissue engineering and neural regeneration.[61,69–72] In addition, p19 stem cells proliferate, which allow for easily examining cell viability, in addition to assessing neurite outgrowth. Lastly, stem cell lines do not have the sterility concerns or the acquisition of fibroblasts as primary cells have following dissection.

It is known that nerve cells require multiple cues (biophysical, biochemical, bioelectrical) for regeneration.[71] While biophysical surface topographies such as fibers, tubes, and grooves[18] and biochemical cues such as growth factors are widely used to control nerve growth, there are only a handful of papers that examined the effects of electrical stimulation on nerve cells *in vitro*. Electrical stimulation may be a promising option for nerve regeneration due to the conductive properties of nervous tissue. In the present work we applied both biophysical and bioelectrical approaches and assessed the contributions of each towards axon alignment and axon outgrowth. Nerve axon alignment was increased on patterned films in comparison to flat films, and axon outgrowth increased in neurons exposed to alternating current (AC) stimulation. Over time, detachment of neurons from the

silk surface occurred, decreasing average axon length and total nerve tissue. As a result, additional surface coatings for long term nerve cell attachment will be important.

Silk films with patterns improved neural alignment, while electrodes increased neurite outgrowth. P19 neurons in electrode fields exhibited less organization compared to the non-stimulated controls. This is reasonable as electrode position, electrode size, electrode shape, and the applied electric field strength are critical factors for determining cell alignment.[64] In future studies, additional investigation are needed into the combination of these electrode parameters to provide optimal outgrowth and alignment with patterned films.

### Mechanism

Electrical stimulation has been reported to enhance neural regeneration through increasing remyelination, guiding extracellular matrix deposition, and increasing axon outgrowth.[73–75] Several electric field-tissue interactions have been suggested toward this goal, including altering pH, Joule heating, mechanical stress, altering membrane potential, or altering receptor expression.[76–78] It has also been hypothesized that electrical stimulation of neurons increases endogenous neurotrophic factor release, which activates regenerative pathways and signaling cascades. For example, it has been reported that electrical stimulation activates endogenous brain derived neurotrophic factor (BDNF) release in hippocampal neurons and increases endogenous nerve growth factor (NGF) release in cultured Schwann cells[74,75], and as a result, activates cell membrane receptors. It is well known that NGF activates the tyrosine kinase receptor A (Trk-A) and BDNF activates the tyrosine kinase receptor B (Trk-B) on the neural cell membrane. The p75NTR receptor, a low affinity binding receptor, is also activated in the presence of several neurotrophins, including NGF and BDNF.[79,80]

To increase neural regeneration pathways downstream, the Trk-A receptor activates intracellular phosphorylation of Src-homologous and collagen like protein (Shc) and tyrosine residues known to signal two major pathways, the phosphoinositide 3-kinases (PI-3K)/Akt pathway and the MEK-mitogen activated protein kinase (MAPK) pathway.[80] The PI-3K protein is a target of the small guanine nucleotide binding protein, Ras, and PI-3 kinase has been demonstrated as a survival protein among neurons.[80] The MEK/MAPK pathways are known to promote synaptic plasticity, long-term potentiation, and are central mediators in axon sprouting and neural differentiation.[80–82] Activation of the Trk-B receptor activates intracellular phosphorylation of Shc that activates the MAPK pathway and push actin filaments (f-actin) in the growth cone outwards.[82]

Additional neural receptors that may be activated by electrical stimulation for neural regeneration include the calcium channel and the two pore domain potassium (2-PK) channel.[74,75,83–85] Specifically, it has been reported that electric fields may regulate phosphorylation of protein kinase A (PKA) and protein kinase C (PKC) which regulate the 2-PK channel.[83] Electric fields may also increase intracellular calcium production and release through neuron calcium channels.[74] Increase in NGF production during electrical stimulation treatments was dependent upon this increase in calcium production.[74] These receptors and pathways potentially activated by electrical stimulation are shown in Figure 9.

## Experimental

### Fabrication of Flat & Patterned Silk Electronic Films (E-Films)

Silk Fibroin Purification - Silk fibroin solution was extracted from Japanese *Bombyx mori* cocoons as described previously.[86,87] Briefly, cocoons from the silkworm were cut, boiled for 30 minutes in sodium carbonate for sericin removal, washed, and dried overnight. The following day, silk fibers were dissolved in 9.3M lithium bromide at 60°C for 4–6 hours. Dissolved silk solution was injected into 3,500 molecular weight dialysis cassettes (Thermo

Fisher Scientific, Waltham, MA). Dialysis in deionized water was performed over 36 hours resulting in a final solution of 6 – 8% silk fibroin.

Patterned Silk Films - A patterned PDMS mold was prepared by mixing a base and a curing agent (Ellsworth Adhesives, Germantown, WI) in a 9:1 ratio (w/w) then pouring this mixture over the grooved patterned substrate. PDMS was cured at 60°C for 2–3 hours then peeled off from the substrate. For patterned silk film fabrication, 6 – 8% silk fibroin solution was poured onto the grooved PDMS mold and allowed to dry slowly for 1–2 days. Once dried, patterned silk films were peeled off the PDMS mold.

Flat Silk Films - Flat silk films were fabricated by the same technique (as mentioned above) by casting 6 –8% aqueous silk over non patterned smooth PDMS surface and were treated under the same conditions.

Electrode Deposition on Silk Films - An electrode mask (Boston Lasers, Haverhill, MA) was generated by laser etching a pattern into a 2.7 cm × 4.3 cm × 0.2 cm black delrin slide. The etched mask was secured on top of a silk film. Electrodes were deposited via sputter coating on top of the mask and silk film using a Cressington 208HR Sputter Coater (Watford, England). Following electrode deposition, the electronic-silk films were treated with methanol and dried overnight to induce β-sheet formation. Electrode materials deposited on the silk films included gold, titanium, and platinum/palladium.

## E-Film Characterization

Silk E-Film Thickness – The thickness of the flat and patterned silk e-films was examined using confocal reflectance microscopy.[88] Briefly, the reflectance signal off of the top surface of the silk film and the reflectance signal off of the bottom surface of the silk film were recorded using a depth scan. Film thickness was calculated as the distance between the reflectance signals of the top a bottom film surfaces. Excitation was at 488 nm, emission was at 488 ± 2 nm.

Electrode Conductivity & One-to-One Electrode Correlation - To verify that the electrodes deposited on the silk films were conductive down the length of the electrode and that crosstalk was not observed between the neighboring electrodes, a 1V test signal was applied at one end of each electrode. During all conductivity measurements, electrical contact was made by connecting the voltmeter probe to the gold electrode. For each test signal applied, voltage measurements were taken across 5 areas per electrode and 5 electrodes per film.

Effects of Electrode Thickness - Electrodes were deposited at thicknesses of 25 nm, 75 nm, and 100 nm as measured by the Cressington Thickness Controller (Watford, England). Conductivity measurements were taken across electrodes of 25 nm, 75 nm, and 100 nm thickness. To accomplish this, a small direct current (DC) test signal was applied across the electrodes. Using a voltmeter the potential across the electrodes was measured. The difference between the applied DC test signal and the measured potential was graphed as an average percent of the original signal. Sample size was n = 20. Measurements were taken at 1V, 1 V 20 Hz, and 1 V 1 kHz. The frequency range used to characterize the conductivity of the electronic-patterned films includes the range of electrical stimulation typically used for engineering tissues.[64]

Electronic Silk Film Conductivity in a Hydrated Environment – For the purpose of assessing electrode adhesion to the silk film surface, conductive electronic films having an electrodes with the thickness of at least 75 nm were placed in phosphate buffered saline (PBS) at room temperature. At 1 day, 2 days, 7 days, and 14 days the films were removed from the PBS and allowed to dry overnight. The next day conductivity measurements were taken.

Following measurements, the films were placed back into PBS until the next time point. Measurements were taken at 1V, 1 V 20 Hz, and 1 V 1 kHz at all time points. Conductivity measurements on the electrodes were also taken prior to hydration for the purpose of a baseline measurement. Sample size was n = 20.

### Design of a Patterned Silk E-Film Material Interface & Chamber

For the purpose of holding the silk films down in a hydrated environment, silk films were secured between a circular PDMS well (Figure 5A) and a 24 mm × 30 mm × 0.15 mm cover glass slide through plasma sterilization. For the purpose of interfacing electronic silk films with an external stimulator, a 99.95% gold wire (Surepure Chemetals, Florham Park, NJ), 100 μm in diameter, was cut 8 cm long and attached to the electronic silk film using a conductive silver paste (Ted Pella, Redding, CA). The silver paste was allowed to dry overnight. The following day the electronic silk film with the external gold wire interface was placed into a 60 mm cell culture dish. The external gold wire and silver adhesive interface was secured in silicon aquarium glue (PETCO, San Diego, CA). The entire silk film interface was allowed to dry at room temperature for at least two days.

As an alternative interface, based on the application of silk proteins as adhesives, e-gel [59] was used in place of silver paste for electrode attachment to e-films. The e-gel was formed by exposing a 25% concentrated silk solution to a 5 V electric field for 10 – 15 minutes. Following gelation, the e-gel was collected in a syringe and applied as glue to attach the gold wire to the electrode films. The e-gel material interface was allowed to dry overnight. Conductivity measurements were taken across the e-gel and silver paste material interface, with and without the chambers. Sample size was n = 20.

### Silk Film Surface Preparation

E-film chambers were soaked in ethanol for 1 hour, washed 4 times with PBS, then exposed to ultraviolet light overnight in a laminar flow hood. Following sterilization, the silk films were soaked for 1 hour in 1 mM laminin (Sigma-Aldrich, St. Louis, MO). After 1 hour, the laminin solution was aspirated and neuron culture media was added to the chamber.

### Cell Culture

P19 stem cells (ATCC, Manassas, VA), originating for a mouse embryonic carcinoma cell line, were expanded in culture at a density of 5,000 cells/$cm^2$ using minimum essential media (Invitrogen Corp., Grand Island, NY) consisting of 7.5% calf serum (Thermo Fisher Scientific, Waltham, MA), 2.5% fetal bovine serum (Invitrogen Corp.), and 0.1% penicillin-streptomycin (Invitrogen Corp.). Stem cells were incubated at 37°C in 5% $CO_2$. Media was changed two times per week. All experiments used stem cell passage numbers between P1–P3.

P19 stem cells were plated at 5,000 cells/$cm^2$ into non-adherent dishes (Sigma-Aldrich, St. Louis, MO) using expansion medium containing 0.5 μM retinoic acid (Sigma-Aldrich, St. Louis, MO). On day three, floating p19 aggregates undergoing differentiation were collected and separated into a single cell suspension using 0.25% trypsin-ethylenediaminetetraacetic acid (EDTA) and a polished glass Pasteur pipette tip. Single cells were replated into non-adherent dishes containing expansion media and 0.5 μM retinoic acid. On day 5, differentiated aggregates were collected, separated into single cells, and plated onto silk films at a density of 100,000 neurons/$cm^2$. To remove non neural differentiated cells, 5 μg/ml cytosine arabinoside was added the following day.[89,90] Media was changed two times per week. Retinoic acid differentiates p19 stem cells into neurons by initiating transcription of target neuronal genes including sonic hedgehog, paired box 6 (pax-6), achaete-scute

complex homolog 1 (mash-1), and wingless-type mouse mammary tumor virus integration site family, member 1 (wnt-1).[91]

### Cell Viability on Electronic Patterned Silk Film

For assessing cell viability on e-films, alamarBlue® (Invitrogen Corp, Grand Island, NY) was used to examine cell proliferation following plating. The alamarBlue® assay was completed as described previously.[24] Briefly, a 9:1 (v/v) dilution of alamarBlue® to neuronal culture medium was added to the samples and allowed to incubate for 2.5 hours. Following incubation, 100 μL of the media in each sample was pipetted into a 96 well plate. Fluorescence measurements, reported in arbitrary units (A.U.), were taken of the media at 560 nm excitation, 590 nm emission. To obtain cell numbers, a standard curve, that measured fluorescence from the reduction of alamarBlue® in wells containing a known number of cells, was used. Sample size per group per time point was n = 3. Three replicates per sample were measured. Results were graphed as the mean ± one standard deviation. As a control, results were compared to neurons seeded on silk films without electrodes.

### Electric Field Modeling

Electric field strength modeling across silk e-films was completed using the electrostatics module for stationary objects in COMSOL Multiphysics® (Burlington, MA), version 4.2, software. COMSOL Multiphysics® approximates partial differential equations by finite element analysis methods. Electric field strength was calculated through equations:

$$\nabla \cdot \boldsymbol{D}=\rho;\boldsymbol{D}=\varepsilon_0\varepsilon_r\mathbf{E};\boldsymbol{E}=-\nabla \boldsymbol{V};$$

where **D** = electric field flux (V m); ρ = free electric charge density; $\varepsilon_0$ = electric constant = $8.85418782\times10^{-12}$ F·m$^{-1}$; $\varepsilon_r$ = dielectric constant; **E** = electric field strength (V/m), **V** = applied max voltage (A Ω). Briefly, the electronic silk films, interface, and chambers were constructed to scale using the geometry feature. E-Film and chamber material properties were either selected from the COMSOL Multiphysics® material library or created for the study using existing material properties in the literature. Materials utilized included, gold, silk, PDMS, glass, p19 neuron culture media, and polystyrene. The material properties were defined as follows: gold (σ = 4.5 *$10^7$ S/m; ρ = 9.0), silk (σ = 16 S/m; ρ = 3.0), glass (σ = 1*$10^{-14}$ S/m; ρ = 4.2), PDMS (σ = 2.59 *$10^{-14}$ S/m; ρ = 2.7), and p19 neuron culture media (σ = 0.431 S/m; ρ = 78), where σ = materials' conductivity and ρ is the materials' electric charge density.[92–94] P19 neuron culture media conductivity was determined from measured values. The waveform applied to the model was a 0.120 V, 1 kHz, sine wave. The geometry was meshed as a coarse free tetrahedral then solved for voltage (V) and electric field strength (V/m).

### Electrical stimulation of neurons

The 99.95% pure gold wire from the chambers were connected to 22 gauge solid wire and placed in parallel with two additional chambers. The chambers sat in one of six wells per tray, which were made from Noryl® (McMaster-Carr, Atlanta, GA). Noryl® has a high melting point, approximately 154°C, and is autoclavable for sterilization purposes. Prior to stimulation, current-voltage measurements were taken across patterned electronic silk films in neuronal culture media. Resistivity was calculated as approximately 1.55 MΩ. Conductivity of neuron culture media across patterned electronic films was calculated as 4.30 mS/cm. The signal applied to each silk film was 120 mV, 1 kHz using a TENMA universal waveform generator (TENMA Test Equipment, Springboro, OH). Voltage applied across each silk film was verified prior to stimulation. Electric field application was performed in the incubator for 45 minutes daily and the experiments ran over 7 days.

Electrical stimulation parameters were based on reports of previous studies.[24,61,64] Experimental groups consisted of patterned electronic silk films, flat electronic silk films, patterned silk films without stimulation, and flat silk films without stimulation.

### Fluorescence Microscopy

An 8 mM calcein acetoxymethyl ester (calcein AM) stock solution (Invitrogen Corp., Grand Island, NY) was mixed with phosphate buffered saline to obtain a 2 μM calcein AM solution. Following solution preparation, cell culture media was aspirated from the patterned electronic silk films, flat electronic silk films, patterned silk films, and flat silk film groups then the 2 μM calcein AM solution was added directly to the cells. Cells were incubated at 37°C for 30 – 45 minutes. Following incubation, the calcein solution was removed from the samples and fresh PBS was added directly to the cells. Cells were imaged with a Leica DMIL fluorescence microscope (Leica, Wetzlar, Germany) with 470 nm ± 20 nm and 525 ± 25 nm filters. Fluorescent images were taken of neurons seeded on patterned electronic silk films, flat electronic silk films, patterned silk films and flat silk films on day 1, day 3, day 5, and day 7. Day 1 was the day following neuron seeding. Images were taken of two different samples per group, per time point. Axon alignment and axon outgrowth were quantified using programs written in MATLAB® (MathWorks, Natick, MA). Axon alignment was calculated as the angle, from 0 – 90 degrees, between the grooved silk surface and axon. An angle of 0 degrees meant that the axon was parallel with the silk film pattern. An angle of 90 degrees meant that the axon was perpendicular to the pattern. Axon alignment was reported as the average angle from the grove on day 1, day 3, day 5, and day 7. Axon alignment was also reported as the percent of total neuron axons lying at every 10 degrees (i.e., 0–10°, 10–20°, 20–30°, 30–40°, 40–50°, 50–60°, 60–70°, 70–80°, 80–90°) from the grove.[56] The relationship of alignment between axons and the direction of neurons seeded on the patterned films was not examined or quantified.

### Immunostaining

Neurons seeded on patterned electronic silk films, flat electronic silk films, patterned silk films and flat silk films were fixed at room temperature for 30 minutes in 4% paraformaldehyde then permeabilized for five minutes in 0.3% triton X-100 and PBS. Following permeabilization, samples were incubated at 37°C for two hours with a primary rabbit anti-mouse β3-tubulin antibody (Sigma-Aldrich, St. Louis, MO) in 10% fetal bovine serum and PBS. Following incubation with the primary antibody, samples were washed three times in PBS then incubated at room temperature for 30 minutes with a secondary antibody, an Alexa Fluor® 568 goat anti-rabbit IgG (Invitrogen Corp, Grand Island, NY). Following incubation of the secondary antibody, samples were washed three times in PBS and imaged in distilled water using a Leica DMIL fluorescence microscope (Leica, Wetzlar, Germany) with 560 nm ± 20 nm and 645 ± 40 nm filters. Staining was completed on day 1, day 3, day 5, and day 7. P19 stem cells seeded on flat silk films were stained and imaged as a negative control. Images were taken of two different samples per group, per time point. Axon outgrowth was quantified and graphed as average length of axon, not including the cell body. The number of axons measured was n = 30 for each group, per time point.

### Statistical Analysis

All quantitative measurements were graphed and reported as the mean ± 1 standard error, $\sigma = \sigma/\sqrt{n}$, unless otherwise noted. Statistical significance was calculated using unpaired two-tailed t-tests with a 95% confidence interval ($p < 0.05$) unless otherwise noted. Statistical significance for axon length was calculated through one-way analysis of variance (ANOVA) followed by Tukey's test for multiple comparisons ($p < 0.05$).

## Conclusions

In conclusion, neural effects from electronic topographical surfaces have not been extensively reported. The present paper provides methods for electrode incorporation onto patterned flexible biomaterial films and options for forming conducting topographical surfaces and electronic-silk film interfaces. The effects of these systems on neuron axons in the presence of electric fields were demonstrated. Examining silk-electronics in different forms such as tubes, scaffolds, and gels may also prove useful for medically-related devices. Finally, different surface topographies may be examined including multi-directional surfaces patterns and nano and micrometer electrospun silk fibers to obtain additional control of outcomes. Probing the mechanistic basis for the responses will also be critical to future optimization of the techniques described here *in vitro* and *in vivo*.

## Acknowledgments

This research was supported by the Armed Forces Institute of Regenerative Medicine (AFIRM) and the Tissue Engineering Resource Center (TERC) through the NIH grant P41EB002520 from the National Institute of Biomedical Imaging and Bioengineering. This work was performed in part at the Center for Nanoscale Systems (CNS), a member of the National Nanotechnology Infrastructure Network (NNIN), which is supported by the National Science Foundation under NSF award no. ECS-0335765. CNS is part of Harvard University.

## References

1. Uebersax L, Mattotti M, Papaloizos M, Merkle H, Gander B, Meinel L. Silk fibroin matrices for the controlled release of nerve growth factor (NGF). Biomaterials. 2007; 28(30):4449–4460. [PubMed: 17643485]
2. Hill PS, Apel PJ, Barnwell J, Smith T, Koman LA, Atala A, Van Dyke M. Repair of peripheral nerve defects in rabbits using keratin hydrogel scaffolds. Tissue Eng Part A. 2011; 17(11–12):1499–505. [PubMed: 21275820]
3. Potucek, R.; Kemp, S.; Syed, N.; Midha, R. Chapter 10 Peripheral Nerve Injury, Repair, and Regeneration. Springer-Verlag New York, LLC; 2009.
4. Belkas J, Shoichet M, Midha R. Peripheral nerve regeneration through guidance tubes. Neurol Res. 2004; 26(2):151–160. [PubMed: 15072634]
5. Witzel C, Rohde C, Brushart T. Pathway sampling by regenerating peripheral axons. J Comp Neuro. 2005; 485(3):183–190.
6. Murakami T, Fujimoto Y, Yasunaga Y, Ishida O, Tanaka N, Ikuta Y, Ochi M. Transplanted neuronal progenitor cells in a peripheral nerve gap promote repair. Brain Res. 2003; 974(12):17–24. [PubMed: 12742620]
7. Lari, H.; Hashim, B.; Qian, H.; Chua, J.; Haas, J. Nerve Regeneration. Providence: Brown University; 2001.
8. Pan H, Cheng F, Chen C, Lai S, Lee C, Yang D, Chang M, Ho S. Post-injury regeneration in rat sciatic nerve facilitated by neurotrophic factors secreted by amniotic fluid mesenchymal stem cells. J Clin Neurosci. 2007; 14(11):1089–1098. [PubMed: 17954375]
9. Pan H, Yang D, Chiu Y, Lasi S, Wang Y, Chang M, Cheng F. Enhanced regeneration in injured sciatic nerve by human amniotic mesenchymal stem cell. J Clin Neurosci. 2006; 13(5):570–575. [PubMed: 16769515]
10. Pollock M. Nerve regeneration. Curr Opin Neurol. 1995; 8(5):354–358. [PubMed: 8542039]
11. Leach M, Feng Z, Gertz C, Tuck S, Regan T, Naim Y, Vincent A, Corey J. The culture of primary motor and sensory neurons in defined media on electrospun poly-L-lactide nanofiber scaffolds. J Vis Exp. 2011:48.
12. Hong S, Kim G. Electrospun micro/nanofibrous conduits composed of poly(epsilon-caprolactone) and small intestine submucosa powder for nerve tissue regeneration. J Biomed Mater Res B Apply Biomat. 2010; 94(2):421–428.

13. Gomez N, Lu Y, Chen S, Schmidt C. Immobilized nerve growth factor and microtopography have distinct effects on polarizatoin versus axon elongation in hippocampal cells in culture. Biomaterials. 2007; 28(2):271–284. [PubMed: 16919328]
14. Clarke J, Tuft B, Clinger J, Levine R, Fiqueroa L, Allan Guymon C, Hansen M. Micropatterned methacrylate polymers direct spiral ganglion neurite and schwann cell growth. Hear Res. 2011; 278(1–2):96–105. [PubMed: 21616131]
15. Brunetti V, Maiorano G, Rizzello L, Sorce B, Sabella S, Cingolani R, Pompa P. Neurons sense nanoscale roughness with nanometer sensitivity. Proc Acad Sci USA. 2010; 107(14):6264–6269.
16. Fozdar D, Lee J, Schmidt C, Chen S. Selective axonal growth of embryonic hippocampal neurons according to topographic features of various sizes and shapes. Int J Nanomedicine. 2010; 6:45–57. [PubMed: 21289981]
17. Fozdar D, Lee J, Schmidt C, Chen S. Hippocampal neurons respond uniquely to topographies of various sizes and shapes. Biofabrication. 2010; 2(3):035005. [PubMed: 20823503]
18. Hoffman-Kim D, Mitchel J, Bellamkonda R. Topography, cell response, and nerve regeneration. Annu Rev Biomed Eng. 2010; 12:203–231. [PubMed: 20438370]
19. Brighton C, Wang W, Clark C. Up-regulation of matrix in bovine articular cartilage explants by electric fields. Biochem Biophys Res Commun. 2006; 342(2):556–561. [PubMed: 16487926]
20. Akanji O, Lee D, Bader D. The effects of direct current stimulation on isolated chrondrocytes seeded in 3D agarose constructs. Biorheology. 2008; 45(3–4):229–243. [PubMed: 18836227]
21. Diniz P, Shomura K, Soejima K, Ito G. Effects of pulsed electomagnetic field (PEMF) stimulation on bone tissue like formation are dependent on the maturation stages of the osteoblasts. Bioelectromagnetics. 2002; 23(5):398–405. [PubMed: 12111759]
22. Fassina L, Visai L, Benazzo F, Bennedetti L, Calligaro A, De Angelis M, Farina A, Maliardi V, Margenes G. Effects of electromagnetic stimulation on calcified matrix production by SAOS-2 cells over a polyurethane porous scaffold. Tissue Eng. 2006; 12(7):1985–1999. [PubMed: 16889527]
23. Ijiri K, Matsunaga S, Fukuyama K, Maeda S, Sakou T, Kitano M, Senba I. The effect of pulsing electromagnetic field on bone ingrowth into a porous coated implant. Anticancer Res. 1996; 16(5A):2853–2856. [PubMed: 8917397]
24. Hronik-Tupaj M, Rice W, Cronin-Golomb M, Kaplan D, Georgakoudi I. Osteoblastic differentiation and stress response of human mesenchymal stem cells exposed to alternating current electric fields. Biomed Eng Online. 2011; 10(1):9. [PubMed: 21269490]
25. Sun S, Liu Y, Lipsky S, Cho M. Physical manipulation of calcium oscillations facilitates osteodifferentiation of human mesenchymal stem cells. FASEB J. 2007; 21(7):1472–1480. [PubMed: 17264165]
26. Sun L, Hsieh D, Yu T, Chiu H, Lu S, Luo G, Kuo T, Lee O, Chiou T. Effect of pulsed electromagnetic field on the proliferation and differentiation potential of human bone marrow mesenchymal stem cells. Bioelectromagnetics. 2009; 30(4):251–260. [PubMed: 19204973]
27. Blumenthal N, Ricci J, Breger L, Zychlinsky A, Solomon H, Chen G, Dorfman R. Effects of low-intensity AC and/or DC electromagnetic fields on cell attachment and induction of apoptosis. Bioelectromagnetics. 1997; 18(3):264–272. [PubMed: 9096845]
28. Sun S, Titushkin I, Cho M. Regulation of mesenchymal stem cell adhesion and orientation in 3D collagen scaffold by electrical stimulus. Bioelectrochemistry. 2006; 69(2):133–141. [PubMed: 16473050]
29. Gordon T, Udina E, Verge V, de Chaves E. Brief electrical stimulation accelerates axon regeneration in the peripheral nervous system and promotes sensory axon regeneration in the central nervous system. Motor Control. 2009; 13(4):412–441. [PubMed: 20014648]
30. Gordon T, Sulaiman O, Ladak A. Chapter 24: electrical stimulation for improving nerve regeneration: where do we stand? Int Rev Neurobiol. 2009; 87:433–444. [PubMed: 19682653]
31. Gordon T, Amirjani N, Edwards D, Chan K. Brief post-surgical electrical stimulation accelerates axon regeneration and muscle reinnervation without affecting the functional measures in carpal tunnel syndrome patients. Exp Neurol. 2010; 223(1):192–202. [PubMed: 19800329]

32. Alrashdam M, Sung M, Kim Kwon Y, Chung H, Kim S, Lee J. Effects of combining electrical stimulation with BDNF gene transfer on the regeneration of crushed rat sciatic nerve. Acta Neurochir (Wien). 2011; 153(10):2021–2029. [PubMed: 21656118]
33. Kemp S, Walsh S, Midha R. Growth factor and stem cell enhanced conduits in peripheral nerve regeneration and repair. Neurol Res. 2008; 30(10):1030–1038. [PubMed: 19079977]
34. Madduri S, Feldman K, Tervoort T, Papaloizos M, Gander B. Collagen nerve conduits releasing the neurotrophic factors GDNF and NGF. J Control Release. 2010; 143(2):168–174. [PubMed: 20035811]
35. Lutolf M, Gilbert P, Blau H. Designing materials to direct stem-cell fate. Nature. 2009; 462(7272): 433–441. [PubMed: 19940913]
36. Place E, Evans N, Stevens N. Complexity in biomaterials for tissue engineering. Nat Mater. 2009; 8(6):457–470. [PubMed: 19458646]
37. Mitragotri S, Lahann J. Physical approaches to biomaterial design. Nat Mater. 2009; 8(1):15–23. [PubMed: 19096389]
38. Yang Y, Chen X, Ding F, Zhang P, Liu J, Gu X. Biocompatibility evaluation of silk fibroin with peripheral nerve tissues and cells in vitro. Biomaterials. 2007; 28(9):1643–1652. [PubMed: 17188747]
39. Lin Y, Ramadan M, Hronik-Tupaj M, Kaplan D, Philips B, Sivak W, Rubin J, Marra K. Spatially controlled delivery of neurotrophic factors in silk fibroin-based nerve conduits for peripheral nerve repair. Ann Plast Surg. 2011; 67(2):147–155. [PubMed: 21712696]
40. Ghaznavi A, Kokai L, Lovett M, Kaplan D, Marra K. Silk fibroin conduits: a cellular and functional assessment of peripheral nerve repair. Ann Plast Surg. 2011; 66(3):273–279. [PubMed: 21263296]
41. Wilz A, Pritchard E, Li T, Lan J, Kaplan D, Boison D. Silk polymer-based adenosine release: therapeutic potential for epilepsy. Biomaterials. 208; 29(26):3609–3616. [PubMed: 18514814]
42. Szybala C, Pritchard E, Lusardi T, Li T, Wilz A, Kaplan D, Boison D. Antiepileptic effects of silk-polymer based adenosine release in kindled rats. Exp Neurol. 2009; 219(1):126–135. [PubMed: 19460372]
43. Pritchard E, Szybala C, Boison D, Kaplan D. Silk fibroin encapsulated powder reservoirs for sustained release of adenosine. J Control Release. 2010; 144(2):159–167. [PubMed: 20138938]
44. Benfenati V, Toffanin S, Capelli R, Camassa L, Ferroni S, Kaplan D, Omenetto F, Muccini M, Zamboni R. A silk platform that enables electrophysiology and targeted drug delivery in brain astroglial cells. Biomaterials. 2010; 31(31):7883–7891. [PubMed: 20688390]
45. Altman G, Diaz F, Jakuba C, Calabro T, Horan R, Chen J, Lu H, Richmond J, Kaplan D. Silk-based biomaterials. Biomaterials. 2003; 24(3):401–416. [PubMed: 12423595]
46. Panilaitis B, Altman G, Chen J, Jin H, Karageorgiou V, Kaplan D. Macrophage responses to silk. Biomaterials. 2003; 24(18):3079–3085. [PubMed: 12895580]
47. Sundar S, Kundu J, Kundu S. Biopolymeric nanoparticles. Sci Technol Adv Mater. 2010; 11:13.
48. Tsioris K, Raja W, Pritchard E, Panilaitis B, Kaplan D, Omenetto F. Fabrication of silk microneedles for controlled-release drug delivery. Adv Funct Mater. 2011; 22(2):330–335.
49. Kim J, Kang G, Nam Y, Choi Y. Surface-modified microelectrode array with flake nanostructure for neural recording and stimulation. Nanotechnology. 2010; 21(8)
50. Zhou C, Confalonieri F, Medina N, Zivaonivic Y, Eshault C, Yang T, Jacquet M, Janin J, Duguet M, Perasso R, et al. Fine organization of bombyx mori fibroin heavy chain gene. Nucleic Acids Res. 2000; 28(12):2413–2419. [PubMed: 10871375]
51. Sofia S, McCarthy M, Gronowicz G, Kaplan D. Functionalized silk-based biomaterials for bone formation. J Biomed Mater Res. 2001; 54(1):139–148. [PubMed: 11077413]
52. Kipke, D.; Shain, W. Microfabricated Silicon Probes for Interfacing with the Nervous System: Examples and Design Considerations. Ann Arbor: University of Michigan; 2010 May-May.
53. Tao H, Kaplan D, Omenetto F. Silk materials-a road to sustainable high technology. Adv Mater. 2012; 24(21):2824–2837. [PubMed: 22553118]

54. Kim D, Viventi J, Amsden J, Xiao J, Vigeland L, Kim Y, Blanco J, Panilaitis B, Frechette E, Contreras D, et al. Dissolvable films of silk fibroin for ultrathin conformal bio-integrated electronics. Nat Mater. 2010; 9(6):511–517. [PubMed: 20400953]
55. Kim D, Kim Y, Amsden J, Panilaitis B, Kaplan D, Omenetto F, Zakin M, Rogers J. Silicon electronics on silk as a path to bioresorbable, implantable devices. Appl Phys Lett. 2009; 95(13): 133701. [PubMed: 20145699]
56. Gil E, Park S, Marchant J, Omenetto F, Kaplan D. Response of human corneal fibroblasts on silk film surface patterns. Macromol Biosci. 2010; 10(6):664–673. [PubMed: 20301120]
57. Lu Q, Wang X, Hu X, Cebe P, Omenetto F, Kaplan D. Stabilization and release of enzymes from silk films. Macromol Biosci. 2010; 10(4):359–368. [PubMed: 20217856]
58. Lawrence B, Wharram S, Kluge J, Leisk G, Omenetto F, Rosenblatt M, Kaplan D. Effects of hydration on silk film material properties. Macromol Biosci. 2010; 10(4):393–403. [PubMed: 20112237]
59. Yucel T, Kojic N, Leisk G, Lo T, Kaplan D. Non-equilibrium silk fibroin adhesives. J Struct Biol. 2010; 170(2):406–412. [PubMed: 20026216]
60. Peignot P, Rhodes K. Choosing a silicone adhesive and treatment system. Med Device Technol. 2004; 15(3):22–24. [PubMed: 15255533]
61. Koppes A, Seggio A, Thompson D. Neurite outgrowth is significantly increased by the simultaneous presentation of schwann cells and moderate exogenous electric fields. J Neural Eng. 2011; 8(4):046023. [PubMed: 21712572]
62. Xu J, Wang W, Clark C, Brighton C. Signal transduction in electrically stimulated articular chondrocytes invovles translocation of extracellular calcium through voltage-gated channels. Osteoarthritis Cartilage. 2009; 17(3):397–405. [PubMed: 18993082]
63. Dube, J.; Methot, S.; Moulin, V.; Goulet, D.; Bourdage, M.; Auger, F.; Germain, L. External electric fields induce morphological changes on human skin cells cultured in vitro. USRI; 2005.
64. Hronik-Tupaj M, Kaplan D. A review of the responses of 2D and 3D engineered tissues to electric fields. Tissue Eng Part B Rev. 2012; 18(3):167–180. [PubMed: 22046979]
65. Tandon N, Goh B, Marsano A, Chao P, Montouri-Sorrentino C, Gimble J, Vunjak-Novakovic G. Alignment and elongation of human-derived stem cells in response to direct-current electrical stimulation. Conf Proc IEEE Eng Med Biol Soc. 2009; 1:6517–6521. [PubMed: 19964171]
66. Kandel, E.; Schwartz, J.; Jessell, T. Principles of Neural Science. McGraw-Hill; 2000.
67. Arien-Zakay H, Nagler A, Galski H, Lazarovici P. Neuronal conditioning medium and nerve growth factor induce neuronal differentiation of collagen-adherent progenitors derived from human umbilical cord blood. J Mol Neurosci. 2007; 32(3):179–191. [PubMed: 17873363]
68. Oe T, Nagashima T, Muramoto M, Yamazaki T, Morikawa N, Okitsu O, Nishimura S, Aoki T, Katayama Y, Kita Y. CyclinB2 and BIRC5 genes as surrogate biomarkers for neurite outgrowth in SH-SY5Y subclonal cells. Neuropharmacology. 2006; 50(8):1041–1047. [PubMed: 16574167]
69. Ghasemi-Mobarakeh L, Prabhakaran M, Morshed M, Nasr-Esfahani M, Ramakrishna S. Electrical stimulation of nerve cells using conductive nanofibrous scaffolds for nerve tissue engineering. Tissue Eng Part A. 2009; 15(11):3605–3619. [PubMed: 19496678]
70. Huang Y, Wu H, Tai N, Wang T. Carbon nanotube rope with electrical stimulation promotes the differentiation and maturity of neural stem cells. Small. 2012; 8(18):2869–2877. [PubMed: 22753249]
71. Lee J, Bashur C, Milroy C, Forciniti L, Goldstein A, Schmidt C. Nerve growth factor-immobilized electrically conducting fibrous scaffolds for potential use in neural engineering applications. IEEE Trans Nanobioscience. 2012; 11(1):15–21. [PubMed: 21712166]
72. Lu C, Hsiao Y, Kuo C, Chen P. Electrically tunable organic bioelectronics for spatial and temporal manipulation of neuron-like pheochromocytoma (PC-12) cells. Biochim Biophys Acta. 2012 Epub ahead of print.
73. Graves M, Hassell T, Beier B, Albors G, Irazoqui P. Electricallly mediated neuronal guidance with applied alternating current electric fields. Ann Biomed Eng. 2011; 39(6):1759–1767. [PubMed: 21298344]
74. Huang J, Ye Z, Hu X, Lu L, Luo Z. Electrical stimulation induces calcium-dependent release of NGF from cultured schwann cells. Glia. 2010; 58:622–631. [PubMed: 19998481]

75. Wan L, Zhang S, Xia R, Ding W. Short-term low-frequency electrical stimulation enhanced remyelination of injured peripheral nerves by inducing the promyelination effect of brain-derived neurotrophic factor on schwann cell polarization. J Neurosci Res. 2010; 88(12):2578–2587. [PubMed: 20648648]
76. Greenebaum B, Sisken B. Does direction of induced electric field or current provide a test of mechanism invovled in nerve regeneration. Bioelectromagnetics. 2007; 28(6):488–492. [PubMed: 17486600]
77. Klein J, Tendi E, Dib-Haji S, Fields R, Waxman S. Patterned electrical activity modulates sodium channel expression in sensory neurons. J Neurosci Res. 2003; 74(2):192–198. [PubMed: 14515348]
78. McCaig C. Studies on the mechanism of embryonic frog nerve orientation in a small applied electric field. J Cell Sci. 1989; 93(4):723–730. [PubMed: 2514189]
79. Kiryushko D, Berezin V, Bock E. Regulators of neurite outgrowth: role of cell adhesion molecules. Ann N Y Acad Sci. 2004; 1014:140–154. [PubMed: 15153429]
80. Kaplan D, Milleri F. Neurotrophin signal transduction in the nervous system. Curr Opin Neurobiol. 2000; 10(3):381–391. [PubMed: 10851172]
81. Waetzig V, Herdegen T. MEKK1 controls neurite regrowth after experimental injury by balancing ERK1/2 and JNK2 signaling. Mol Cell Neurosci. 2005; 30(1):67–78. [PubMed: 16006144]
82. Airaksinen M, Saarma M. The GDNF family: signaling, biological functions and therapeutic value. Nat Rev Neuro. 2002; 3:383–394.
83. Mathie A, Kennard L, Veale E. Neuronal ion channels and their sensitivity to extremely low frequency weak electric field effects. Radiat Prot Dosimetry. 2003; 106(4):311–315. [PubMed: 14690272]
84. Mehta A, Halder S, Khanna N, Tandon O, Sharma K. Antagonism of stimulation-produced analgesia by naloxone and n-methyl-d-aspartate: role of opioid and n-methyl-d-aspartate receptors. Hum Exp Toxicol. 2012; 31(1):51–56. [PubMed: 21803783]
85. Saygili E, Schauerte P, Kuppers F, Heck L, Weiss J, Weber C, Schwinger R, Hoffman R, Schroder J, Marx N, et al. Electrical stimulation of sympathetic neurons induces autocrine/paracrine effects of NGF mediated by trkA. J Mol Cell Cardiol. 2010; 49(1):79–87. [PubMed: 20138055]
86. Kim U, Park J, Kim H, Wada M, Kaplan D. Three-dimensional aqueous derived biomaterial scaffolds from silk fibroin. Biomaterials. 2005:26.
87. Kang J, Gimble J, Kaplan D. In vitro 3D model for human vascularized adipose tissue. Tissue Eng Part A. 2009; 15(8):2227–2236. [PubMed: 19207036]
88. Larson B, Abeytunge S, Rajadhyaksha M. Performance off full-pupil line-scanning reflectance confocal microscopy in human skin and oral mucose in vivo. Biomed Opt Express. 2011; 2(7): 2055–2067. [PubMed: 21750780]
89. Mani S, Schaefer J, Meiri K. Targeted disruption of GAP-43 in p19 embryonal carcinoma cells inhibits neuronal differentiation. As well as acquisition of the morphological phenotype. Brain Res. 2000; 853(2):384–395. [PubMed: 10640639]
90. Shen Y, Mani S, Meiri K. Failure to express GAP-43 leads to disruption of a multipotent precursos and inhibits astrocyte differentiation. Mol Cell Neurosci. 2004; 26(3):390–405. [PubMed: 15234344]
91. Ulrich H, Majumder P. Neurotransmitter receptor expression and activity during neuronal differentiation of embryonal carcinoma and stem cells: from basic research towards clinical applications. Cell Prolif. 2006; 39(4):281–300. [PubMed: 16872363]
92. Ishikawa E, Seoung-Kwon B, Miyawakia O, Nakamura K, Shiinoki Y, Ito K. Freezing injury of cultured rice cells analyzed by dielectric measurement. J Ferment Bioeng. 1997; 83:222–226.
93. Hyung-Kew, L.; Sun-Il, C.; Seong-Jin, K.; Kwang-Seok, Y.; Euisik, Y.; KK-H. A modular expandable tactile sensor using flexible polymer. IEEE International Conference on Micro Electro Mechanical Systems; 2005. p. 642-645.
94. Sun J, Vajandar S, Xu D, Kang Y, Hu G, Li D, Li D. Experimental characterization of electrical current leakage in poly (dimethylsiloxane) microfluidic devices. Microfluid Nanfluid. 2009; 6(5): 589–598.

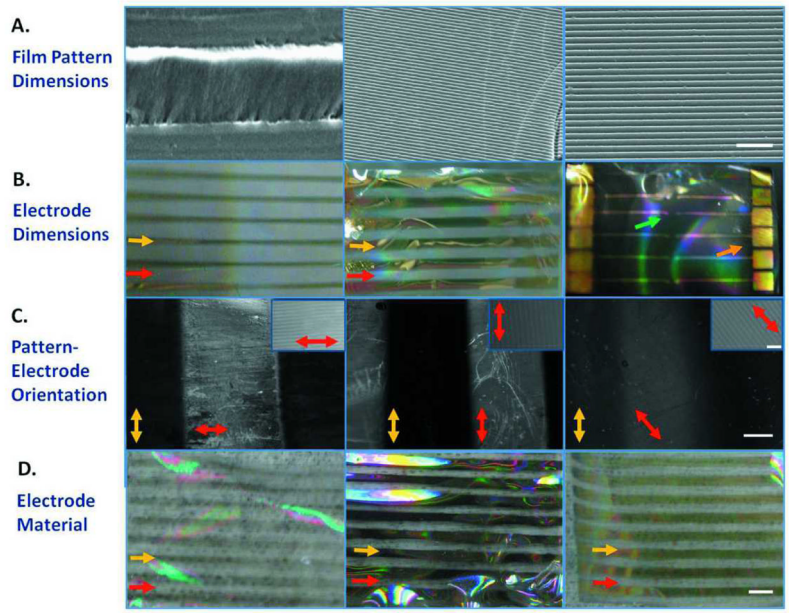


**Figure 1. Electronic Patterned Silk Film Designs**

(a) Patterned Silk Film Dimensions: (left) 40 μm width grooves, (middle) 3.5 μm width grooves having 350 nm depth, and (right) 3.5 μm width grooves having 500 nm depth. Scale bar is 20 μm. (b) Electrode dimensions included (left) 0.5 mm × 4 mm, (middle) 1.0 mm × 4 mm, and (right) 2 $mm^2$ electrode pads with an 8 mm × 50 $\mu m^2$ electrode array. Red arrows are pointing to the silk film. Yellow arrows are pointing to the electrodes. The orange arrow points to the 2 $mm^2$ electrode pads. The green arrow points to the 50 $um^2$ electrode pads. (c) Electrodes are oriented (left) perpendicular, (middle) parallel, or (right) at 45° from the grooved surface patterns. Scale bar is 500 μm. Red arrows mark the clear silk film and are showing the direction of the patterns on the silk film. Yellow arrows mark gold electrodes and are pointing to the direction of the electrodes. Scale bar of silk film patterns in upper right hand corner is 20 μm. (d) Electrode deposition utilizing (left) platinum/palladium, (middle) titanium, and (right) gold. Red arrows are pointing to the silk film. Yellow arrows are pointing to the electrodes. Scale bar is 4 mm.

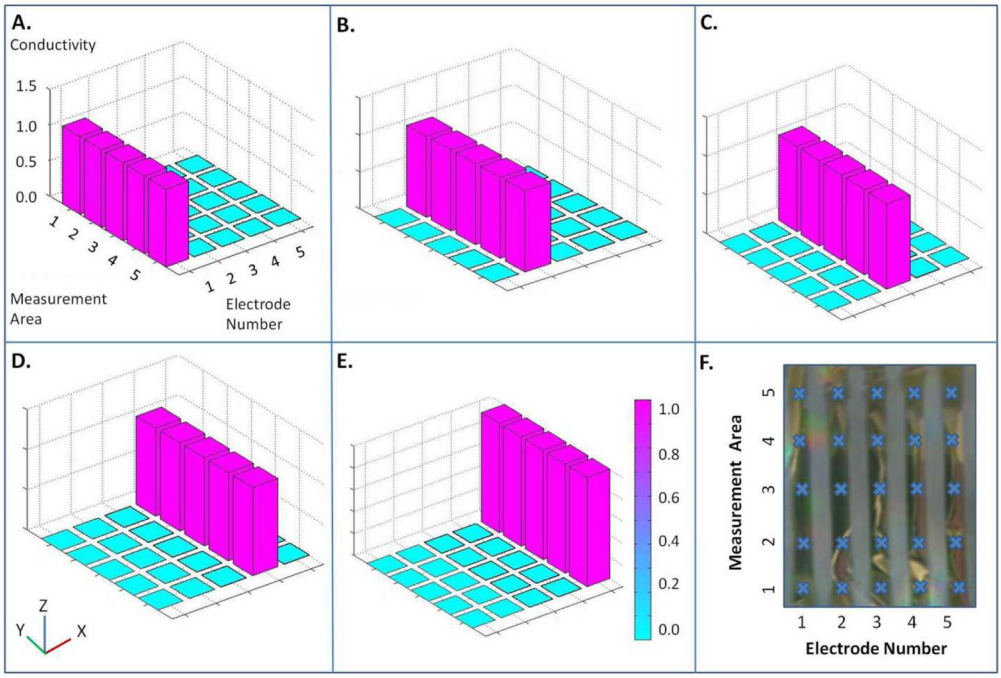


**Figure 2. Electrode Conductivity across Silk Films**

Conductivity measurements on silk e-films in response to (a) Stimulation of electrode #1 (b) Stimulation of electrode #2 (c) Stimulation of electrode #3 (d) Stimulation of electrode #4 (e) Stimulation of electrode #5. (f) Conductivity measurement locations on electronic silk films. Each location is marked with a ‘X’.

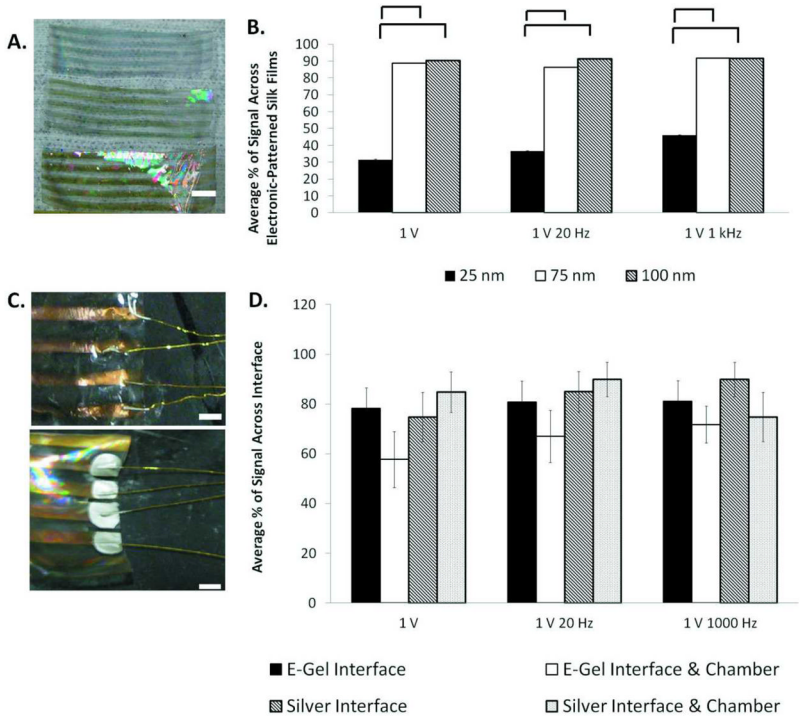


**Figure 3. Conductivity Across Electronic Silk Films**

(a) Images of electrode thickness on silk films at 25 nm (top film), 75 nm (middle film), and 100 nm (bottom film). Scale bar is 10 mm. (b) Conductivity measurements across electronic films at 25 nm, 75 nm, and 100 nm thickness. Statistical significance between groups is marked by a bracket ($p < 0.05$). (c) (top) e-gel interface across silk films and (bottom) silver interface across silk films. Scale is 2 mm. (d) Conductivity across interface and chamber. Statistical significance between groups is marked by an asterisk (* $p < 0.05$).

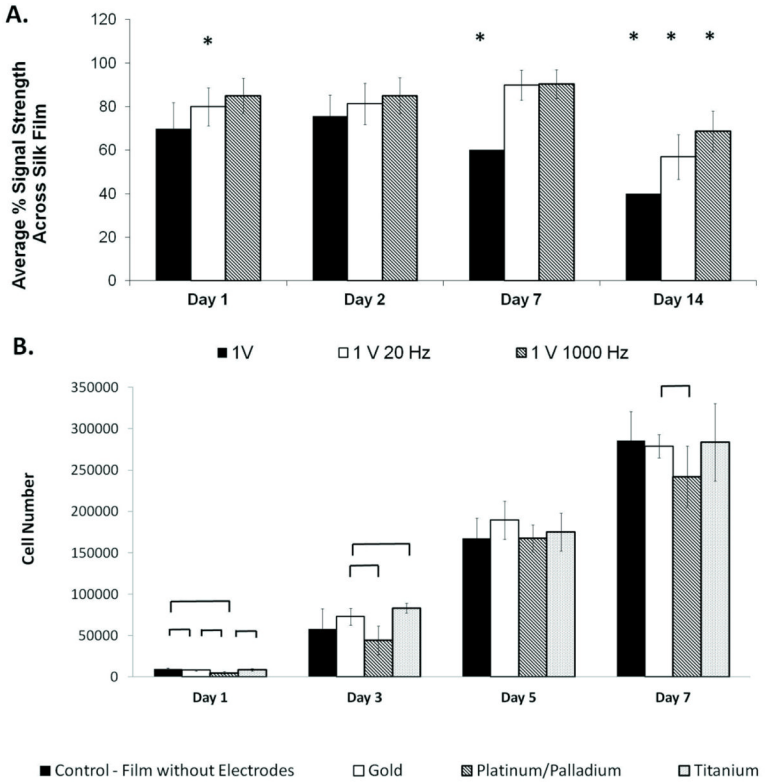


**Figure 4. Time Studies of E-Film Functionality**

(a)Measurements of electrode conductivity at 1 V, 1 V 20 Hz, and 1 V 1 kHz in a hydrated environment over two weeks. Statistical significance is marked by an asterisk ($p < 0.05$) and denotes a statistical difference in electrode conductivity compared to conductivity prior to hydration. (b) Cellular proliferation on day 1, day 3, day 5, and day 7. Groups included p19 cells seeded on silk films without electrodes, platinum palladium electronic silk films, gold electronic silk films, and titanium electronic silk films. Statistical differences in cell number are marked by a bracket ($p < 0.05$).

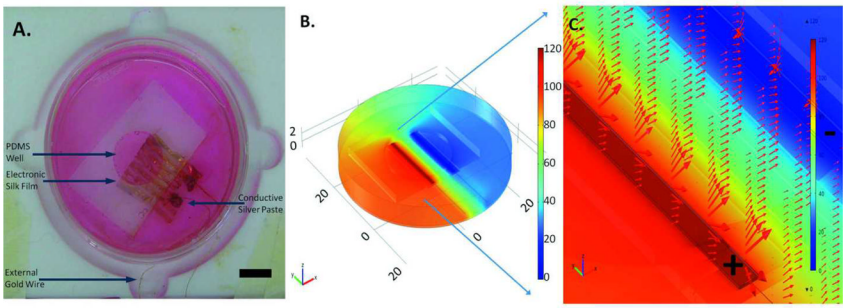


**Figure 5. Electronic Silk Film Modeling**

(a) Image of the modeled electronic silk film and chamber. Scale bar = 1 cm. (b) Maximum voltage applied to the chamber. Color bar is in mV. (c) Electric field strength and electric field direction is illustrated by the red arrows. Electrodes designated as anode and cathode are outlined and then marked by a positive and negative symbol, respectively.

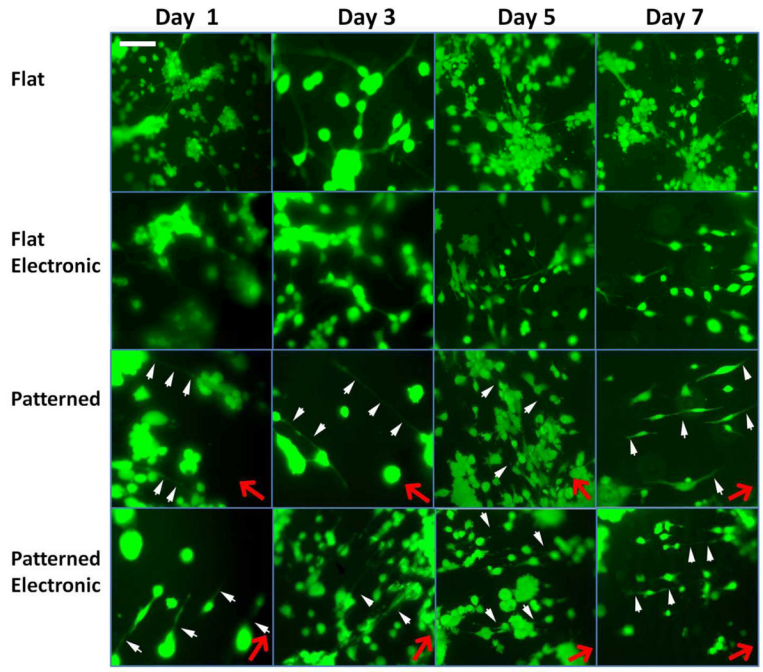


**Figure 6. Fluorescent Microscopy Images**

Fluorescent microscopy images of p19 neurons on flat silk films, flat electronic silk films, patterned silk films, and patterned electronic silk films on day 1, day 3, day 5, and day 7. Pattern direction is noted by the red arrows. Axons aligned in the direction of the pattern are noted by the white arrows. Scale bar is 150 μm.

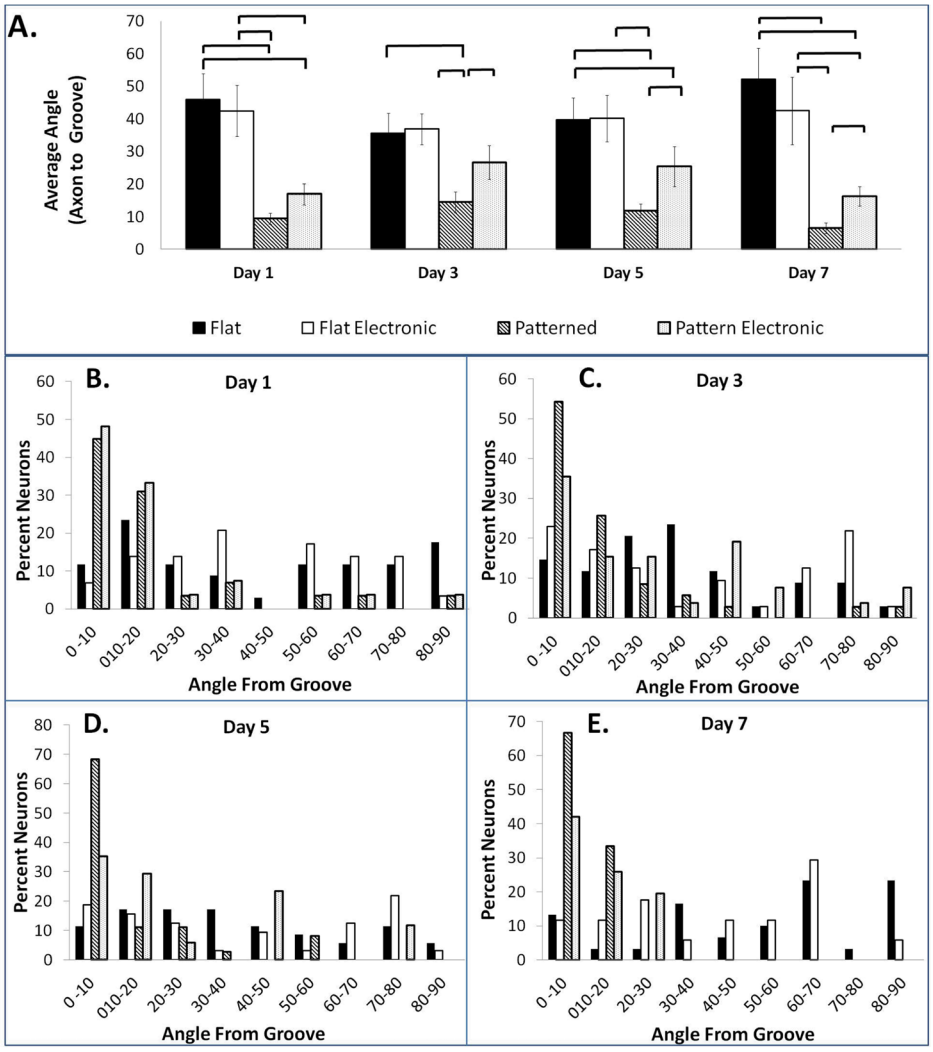


**Figure 7. Quantification of Axon Alignment**

(a) Average axon alignment on day 1, day 3, day 5, and day 7. Statistical significance between groups is marked by a bracket ($p < 0.05$). Quantification of axon alignment on (b) day 1, (c) day 3, (d) day 5, and (e) day 7. Axon alignment on flat silk films, flat electronic silk films, patterned silk films, and patterned electronic silk films is binned within every 10° to provide information on alignment over the neuron population.

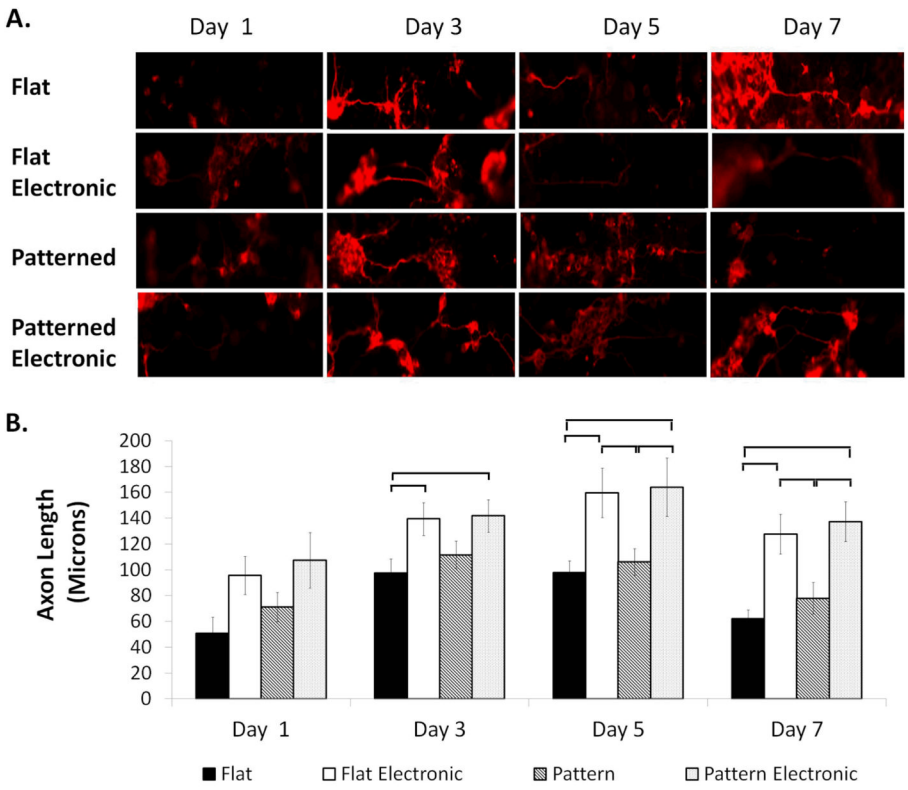


**Figure 8. β3-Tubulin Protein Expression**

(a)Immunofluorescence staining of β3-tubulin expression on day 1, day 3, day 5 and day 7. Scale bar is 75 μm. (b) Average axon outgrowth on day 1, day 3, day 5, and day 7. Statistical significance between groups is marked by a bracket ($p < 0.05$).

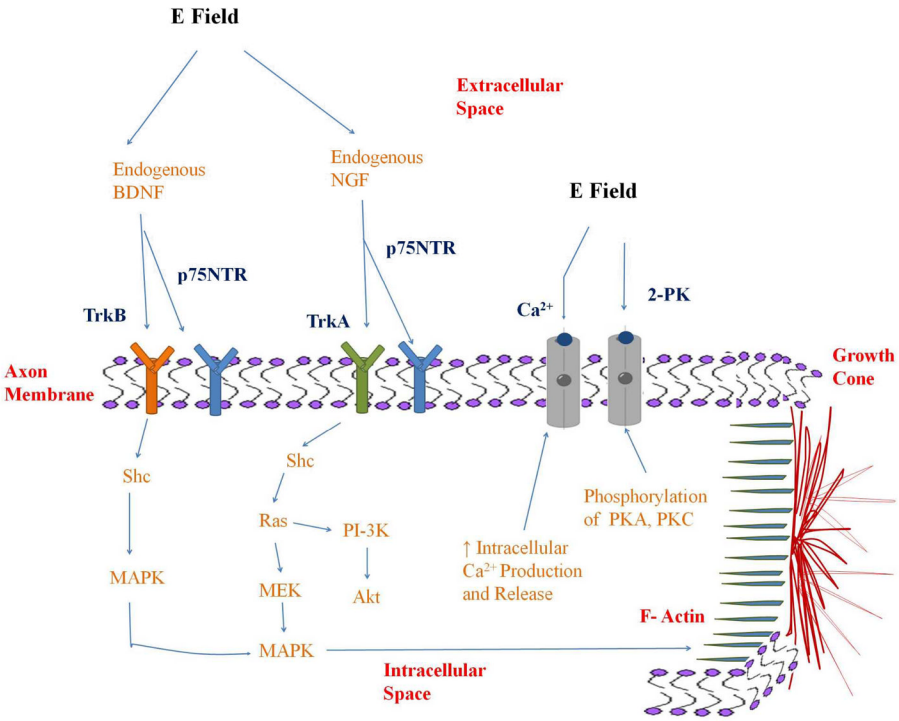


**Figure 9. Mechanisms**

Nerve receptors and regeneration pathways activated through electrical stimulation.